Evaluation of Spent Catalyst Structure Changes during Ethylbenzene Dehydrogenation in Different Technologies

Haghlesan, Amir Naser; Alizadeh, Reza*[+]; Fatehifar, Esmail

Faculty of Chemical Engineering, Sahand University of Technology, PO Box 51335/1996, Tabriz, I.R. IRAN

ABSTRACT: *Ethylbenzene (EB) dehydrogenation to styrene (SM) on an industrial scale is generally performed using classic and SMART (Styrene Monomer Advanced Reheat Technology) technologies. In the current study, spent catalysts structural changes through classic and SMART technologies were investigated and compared with the fresh catalyst. For this purpose, XRF, XRD, SEM-EDX, FT-IR, BET and crushing strength analysis were employed. It was found that styrene production via SMART technology with 40% potassium loss is led to more catalyst deactivation than the classic ones (26%). Due to pore mouth blocking by coke formation, the average pore radius in both classic and SMART spent catalysts is reduced about 33% and 53% compared to the fresh ones, respectively. SEM analysis showed that potassium migration mechanism is related to the temperature gradient in the classic spent catalysts and chemical vapour transportation in the SMART spent catalysts. Comparative evaluation of the catalysts performance indicated that the SMART spent catalyst with about 72% activity loss is more deactivated than the classic ones (61%). The large drop of styrene yield (72-74%) of SMART spent catalyst revealed that the activity is more depending on the pore mouth size, rather than the specific surface area. However, in situ steam injection redistributed migrated potassium and increased the selectivity of the classic spent catalyst, but it was led to more potassium migration and catalyst deactivation in the SMART spent ones. According to this study, styrene production and industrial unit design based on SMART technology not recommended strongly.*

KEYWORDS: *Catalyst deactivation; Ethylbenzene dehydrogenation; SMART technology; Styrene.*

INTRODUCTION

Styrene is one of the most important unsaturated aromatic monomers used in industry to produce polymers, copolymers, tripolymers, etc [1, 2]. The industrial production of styrene was estimated about 25 million tons in 2002, with a significant increase in production expected in the future [3].

About 90% of global styrene industrial production units are using ethylbenzene dehydrogenation technologies. This reaction is endothermic, catalyst relevant and can be completed adiabatically in the gas phase [4]. Ethylbenzene vapors convert to styrene as a result of dehydrogenation along with benzene (BZ) and toluene (TOL), as by-products, in line with the following equations [5].

** To whom correspondence should be addressed.*

+ E-mail: r.alizadeh@sut.ac.ir

Other address of authors: Environmental Engineering Research Center (EERC), Sahand University of Technology, P.O. Box 51335-1996 Tabriz, I.R. IRAN

1021-9986/2017/1/45 13/$/6.30

$$\underset{EB}{C_6H_5-C_2H_5} \xleftrightarrow{Cat.} \underset{SM}{C_6H_5-C_2H_3} + H_2 \quad (1)$$

$$\Delta H = 124.9\,kJ/mol$$

$$\underset{EB}{C_6H_5-C_2H_5} \longrightarrow \underset{BZ}{C_6H_6} + C_2H_4 \quad (2)$$

$$\Delta H = 106.5\,kJ/mol$$

$$\underset{EB}{C_6H_5-C_2H_5} + H_2 \longrightarrow \underset{TOL}{C_6H_5-CH_3} + CH_4 \quad (3)$$

$$\Delta H = -57.1\,kJ/mol$$

Ethylbenzene and steam are mixed in the reactors inlet and ethylbenzene dehydrogenation takes place at a temperature range of 580 to 640 °C with a steam to oil (Ethylbenzene) ratio of 1.3 (wt./wt.). In literature, different roles have been presented for steam such as: supply heat of reaction, increase ethylbenzene conversion, removal of coke from catalyst surface and inhibitor of catalyst deactivation due to Fe_2O_3 reduction [5]. In the conventional dehydrogenation process which is known as classic technology, a heat exchanger has been used between reactors for increasing first reactor outlets temperature for performing dehydrogenation reaction in the second reactor. While, in SMART technology temperature enhancement is carried out by combustion of hydrogen, which produced in the first reactor, by oxygen instead of the heat exchanger.

Industrial ethylbenzene dehydrogenation catalysts are composed of iron oxide (Fe_2O_3) with potassium promoter (10wt.%) and along with molybdenum, cerium, vanadium or tungsten to enhance the selectivity and lifetime of the catalysts [6]. Also, many attempts at using new processes or replacing the different catalysts in the dehydrogenation of ethylbenzene have been successful [7- 9]. According to studies, potassium has a remarkable effect on the enhancement of iron oxide catalyst activity. Besides, alkali doping increases the catalyst efficiency due to gasification of coke and carbonaceous deposits [10]. According to *Mross*'s findings [11], potassium addition (>3wt.%) to iron oxide prevents catalyst shrinkage and density reduction and increases the porosity of the catalyst [11].

Deactivation of ethylbenzene dehydrogenation catalyst in the classic technology, has been attributed to potassium migration to the canter of the catalyst pellet duo to the temperature gradient resulting from the endothermic nature of reaction [12]. Furthermore, catalyst deactivation due to potassium migration was studied by *Matsui et al.* [13] in a differential reactor at constant temperatures. Moreover, the effect of CO_2 on the activity decay of dehydrogenation catalyst has been considered by *Matsui et al.* [14]. They indicated that CO_2 presence in the feed (0.1-0.5 mol%) results in a minor loss in styrene production despite reduction in catalyst deactivation rate

Serafin et al. [15] proposed that 0.25-5wt.% Cr addition to catalyst could induce stability of potassium ferrite ($K_2Fe_{22}O_{34}$) active phase along with enhancement in activation energies of potassium desorption. According to *Bieniasz et al.* [16], catalyst deactivation delay in the presence of Cr is as a result of work function increase and limitations of potassium diffusion from the bulk towards the surface.

Deactivation of ethylbenzene dehydrogenation catalyst over time can occur due to the formation of coke and carbonaceous deposits, potassium migration, Fe^{3+} reduction (Fe_2O_3 reduction to Fe_3O_4) and physical degradation [17, 18]. This process leads to the replacement of the catalyst after nearly two years which is a critical problem from both operational and economic aspects. Despite having interaction between factors that affect deactivation, in ethylbenzene dehydrogenation modeling studies, either the factors have been surveyed independently or their influence has generally been ignored [19-21]. Deactivation of ethylbenzene dehydrogenation catalyst in classic technology has been studied by *Baghalha & Ebrahimpour* [22] and *Shiji et al.* [23]. They compared structure and performance changes in fresh and classic spent catalyst via XRD, SEM, XRF, etc., methods. But there is no comparison between the different styrene production technologies.

The objective of this work was to compare deactivation of ethylbenzene dehydrogenation industrial catalyst via classic and SMART technology for the first time. We expect that the results reported here will lead to choosing the best technology of styrene production and industrial unit designers.

EXPERIMENTAL SECTION

Materials

For conducting catalysts activity tests in pilot scale, commercial ethylbenzene from benzene alkylation unit and demineralized water was used for styrene and production,

Table 1: Oxygen injection rate in the SMART reactor.

EB Feed(m^3/h)	Actual (kg/h)	Design (kg/h)	Deviation (%)
18	731.20	684.26	6.86
19	775.65	722.28	7.39
20	817.84	760.29	7.57
21	863.93	798.31	8.22

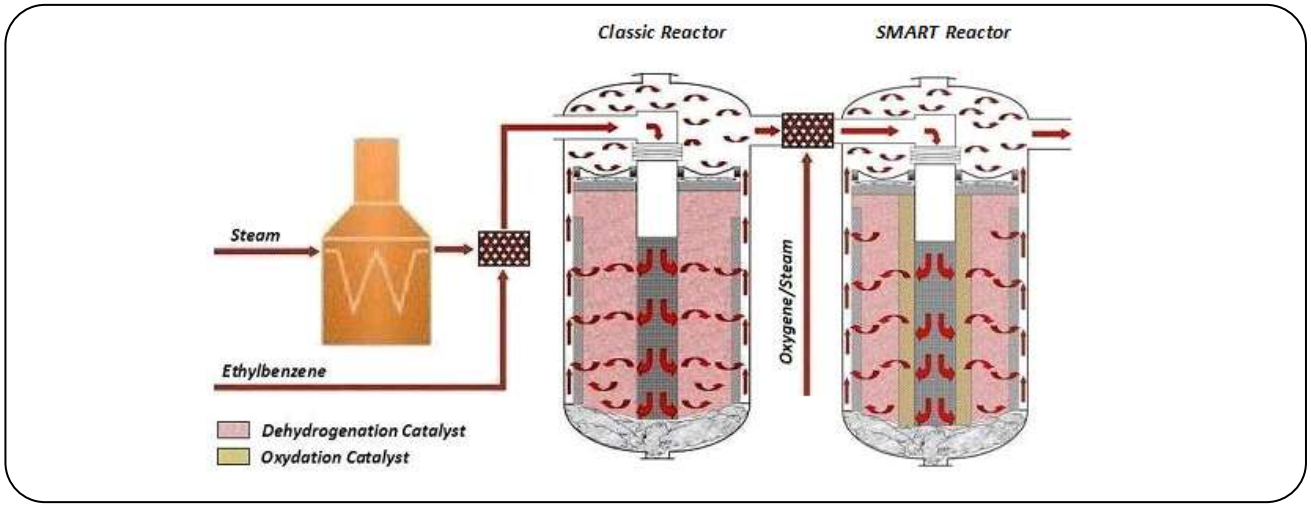

Fig. 1: Schematic of styrene monomer reactors.

respectively. Both of classic and SMART spent catalysts were downloaded from the industrial reactors which had been used for about 36 months under the temperature range of 580 to 640°C, LHSV= 1 hr^{-1} and steam to oil ratio = 1.3 (wt./wt.) condition. The fresh and spent catalysts with a diameter about 3 mm and length of 4-6 mm, are BASF (S6-32) type and mainly contained of Fe_2O_3 and Fe_3O_4, respectively. A schematic representation of the ethylbenzene dehydrogenation reactors is depicted in Fig. 1.

As can be seen in Fig. 1, the SMART reactor catalysts have been run in the presence of oxygen in spite of the classic reactor catalysts. But the designed rate of oxygen injection is not sufficient for increasing the temperature of the first reactor for dehydrogenation reaction to occur. Subsequently, a high rate of oxygen injection is necessary to control the SMART reactor temperature (Table 1).

It seems that the extra oxygen injection affects the SMART spent catalyst structure changes and deactivation mechanism.The feed to this unit is azeotrope mixture of steam, fresh ethylbenzene and recycled unreacted ethylbenzene from third reactor, which is introduced to the first reactor. Afterward, the outlet of the first reactor is mixed with superheated steam, into which the oxygen is injected from oxygen package, and is directed to the second reactor.

Analysis and catalyst characterization

The crystalline phase of catalysts was characterized by x-ray diffractometer (XRD-Siemens D5000) with a Cu. Kα (λ=0.154056 nm) monochromatic radiation at a voltage of 40 kV and a current of 30 mA. Diffraction patterns were obtained in the 2θ range of 20-80° at a scanning rate of 1.2°/min. The average crystalline size was determined by the Scherrer equation as follows:

$$D = \frac{0.9\lambda}{B\cos\theta} \quad (4)$$

Where D is the mean crystallite size, B is the half width at the maximum height (FWHM) of Fe_2O_3, Fe_3O_4, $K_2Fe_{22}O_{34}$ and CeO_2 phases, λ is the wavelength (nm), and θ is the diffraction angle in correspondence to the main diffraction peak. Determination of elements contents was obtained by the X-Ray Florescence (XRF)

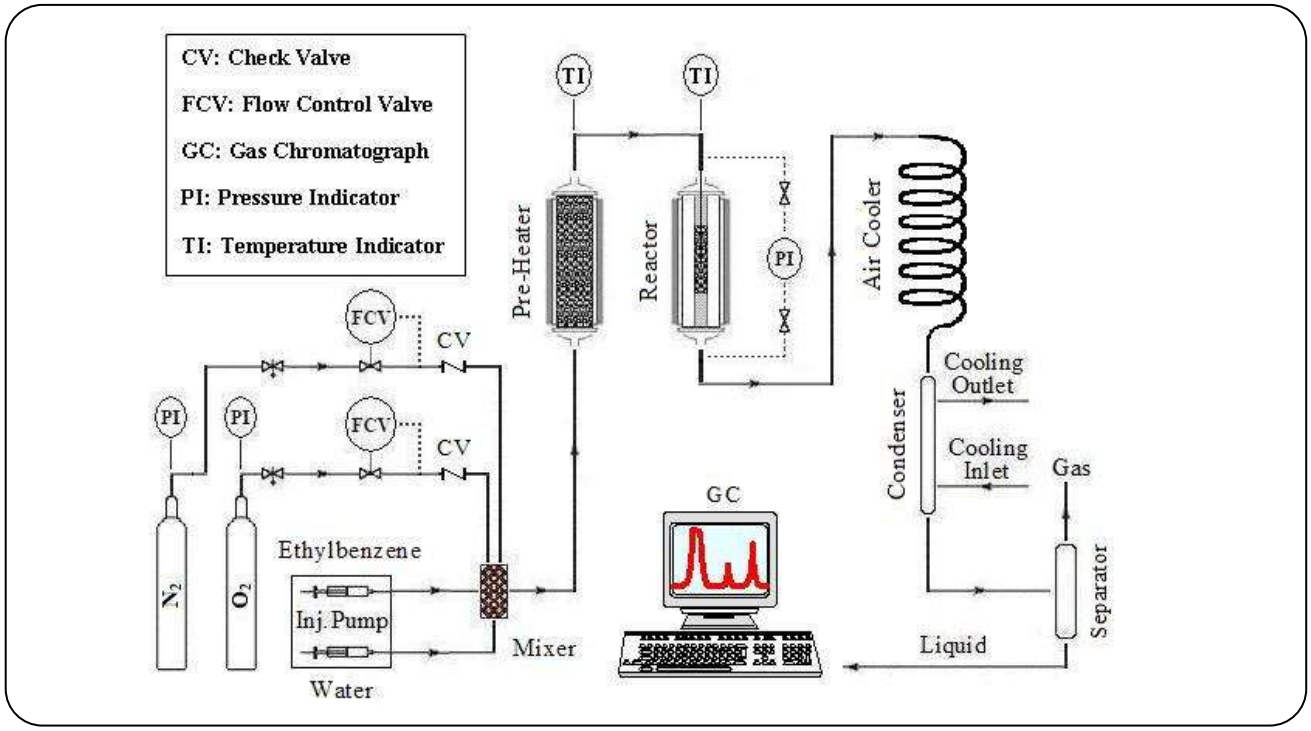

Fig. 2: Experimental setup used for catalyst activity tests.

spectroscopy (Philips MagiX PRO model PW 2540). However, the wet chemical analysis was also used through spectrophotography (Shimadzu UV-3100 S) to verify Fe and potassium contents which were obtained by XRF analysis. Identification of chemical structure and particle size was performed by FT-IR (Unican 4000) and scanning electron microscope (SEM-Tescan Mira3FE SEM), respectively. Potassium line scans were analysed with the CAM SCAN MV 2300 Energy Dispersive X-ray (EDX) spectroscope for all of the catalysts. Moreover, measurement of the surface area and pore size distribution was done by BET methods (Quantachrome NOVA 2000). Besides, grain crushing strength tests was performed by the ASTM 4179 methods

•

Catalyst performance analysis

A laboratory scale fixed-bed reactor (stainless steel - 10 cm length and 1.5 cm I.D.) which was placed inside an electrical furnace was used for determining catalyst activity. The temperature of the pre-heater and furnace was kept constant through a Proportional Integral Derivative (PID) controller. Also water and ethylbenzene injection were carried out by a programmable two channel syringe pump. The reactor effluent was further cooled in the products condenser and separated to the liquid phase and non -condensable gases (off gases) according to Fig. 2. The catalytic activity was evaluated in the temperature ranges of 580 to 640°C under atmospheric pressure. The ratio of reactant to inert flow rates were adjusted to obtain $(EB + H_2O)/(EB + H_2O + N_2) = 0.5$ (vol./vol. in the gas phase), LHSV = 1 hr^{-1} and steam to oil = 1.3 (wt./wt.).

The reactor feed and liquid products were analysed with a Chrompack CP 9001 gas chromatograph equipped with fused silica capillary column (CP-Wax 52 CB 25m, 0.32 mm, 1.2μm) and the FID detector. The gaseous effluents (N_2, O_2, CH_4, C_2H_4, C_2H_6, CO, CO_2) were determined with the CP-Molsieve 5A 25m, 0.53mm, 50μm column and the TCD detector, however, the CP-PoraPLOT Q 50m, 0.53mm, 20μm column and the FID detector were used for ethylbenzene, styrene, benzene, and toluene identification.

In this work, conversion of ethylbenzene, selectivity of the main liquid products and yields of styrene were calculated according to the following formulas:

$$X_{EB}(\%) = \frac{F_{EB(in)} - F_{EB(out)}}{F_{EB(in)}} \times 100 \quad (5)$$

$EB = \text{Ethylbenzene}$

Table 2: Chemical composition of catalyst by XRF spectroscopy.

Component	Fresh	Spent classic	Spent SMART
Fe_2O_3*/ Fe_3O_4*	80.04 ± 0.05	73.97 ± 0.05	74.13 ± 0.05
FeO*	0.00 ± 0.05	8.21 ± 0.05	9.32 ± 0.05
CaO	1.59 ± 0.01	1.37 ± 0.01	1.04 ± 0.01
MgO	0.94 ± 0.01	1.04 ± 0.01	1.14 ± 0.01
K_2O*	8.91 ± 0.05	6.58 ± 0.05	5.27 ± 0.05
MnO	0.43 ± 0.01	0.55 ± 0.01	0.56 ± 0.01
MoO_3	2.07 ± 0.01	1.92 ± 0.01	1.89 ± 0.01
CeO_2	6.02 ± 0.05	6.36 ± 0.05	6.65 ± 0.05

** Also calculated with wet chemical analysis*

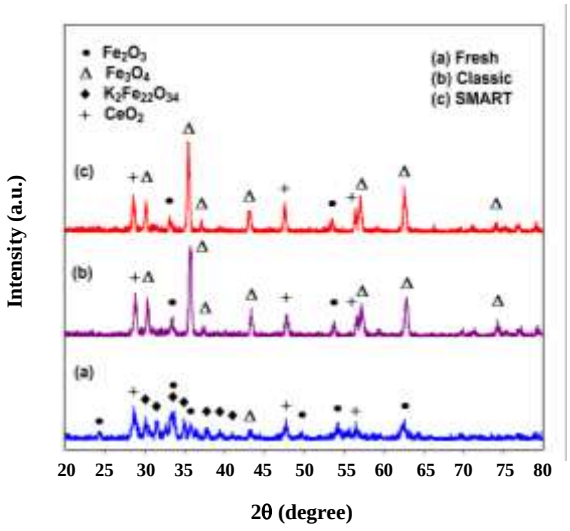

Fig. 3: XRD pattern of fresh and spent catalysts.

$$S_i\,(\%) = \frac{F_{i(out)} - F_{i(in)}}{F_{EB(in)} - F_{EB(out)}} \times 100 \qquad (6)$$

$i \equiv \text{Styrene, Benzene, Toluene}$

$$X_{EB}(\%) = \frac{F_{EB(in)} - F_{EB(out)}}{F_{EB(in)}} \times 100 \qquad (7)$$

$EB = \text{Ethylbenzene}$

Where F is the molar flow rate.

RESULTS AND DISCUSSION

Characterization of the catalysts

XRF and wet chemical analysis results for the catalysts are shown in Table 2. As can be seen, potassium content in the spent catalysts dropped sharply and potassium loss was relevant to styrene production methods so that the styrene production via SMART technology with 40% potassium loss leads to more deactivation than the classic methods (26%).

Ce and Mo concentrations in the spent catalysts were nearly constant due to their higher atomic weight, causing diffusion limitation through the catalyst pellet. Increasing the FeO amount in the spent catalysts is owing to elevated Fe_2O_3 reduction rate which accelerated catalyst deactivation (Eq. (8)). By comparison of the FeO content in the spent catalysts, it can be concluded that the SMART technology leads to more catalyst deactivation.

$$Fe_2O_3 \xrightarrow{H_2} Fe_3O_4 \xrightarrow{H_2} FeO \qquad (8)$$

The XRD patterns and average crystallite size of fresh and spent catalysts are shown in Fig. 3 and Table 3 respectively. As can be observed from the XRD patterns, four phases of Fe_2O_3, Fe_3O_4, $K_2Fe_{22}O_{34}$ and CeO_2 exist. $K_2Fe_{22}O_{34}$ with diffraction peaks at 2θ=30.0, 31.6, 33.8, 35.2, 37.8, 39.9, 41.8 (JCPDS: 00-31-1034) along with Fe_2O_3 with diffraction peaks at 2θ=24.1, 33.2, 35.6, 49.5, 54.0, 62.5 (JCPDS: 00-33-0664) are the dominant crystallite phase in the fresh catalyst. $KFeO_2$ is not detectable easily, and in our results, it was not recognised too, due to transformation into amorphous species in the presence of air and highly diluted. However, $KFeO_2$ could be formed via $K_2Fe_{22}O_{34}$ heating [24-26].

Unlike fresh catalyst, Fe_3O_4 with the diffraction pattern at 2θ=30.4, 35.8, 37.5, 43.5, 57.6, 63.3, 74.9 (JCPDS: 01-75-0449) was the main crystallite phase in spent ones. This result is expectable, because the decrease in Fe_2O_3 content is attributef to Fe^{+3} reductions to Fe^{2+}, and eventually a steady state phase Fe_3O_4 is formed.

Table 3: Structural properties of fresh and spent catalysts.

Catalyst	Crystallite size (nm)				Crystallite phase			
	Fe_2O_3	Fe_3O_4	$K_2Fe_{22}O_{34}$	CeO_2	Fe_2O_3[b]	Fe_3O_4[c]	$K_2Fe_{22}O_{34}$[d]	CeO_2[e]
Fresh	21.1	26.5	26.2	17.4	Cubic	Cubic	Hexagonal	Cubic
Spent classic	30.1	42.4	-	29.8	Cubic	Cubic	-	Cubic
Spent SMART	42.1	53.0	-	41.6	Cubic	Cubic	-	Cubic

a) Crystallite size was estimated by Scherre's equation. b) Reference code (JCPDS): 00-33-0664.
c) Reference code (JCPDS): 01-75-0449. d) Reference code (JCPDS): 00-31-1034.
e) Reference code (JCPDS): 01-075-0076.

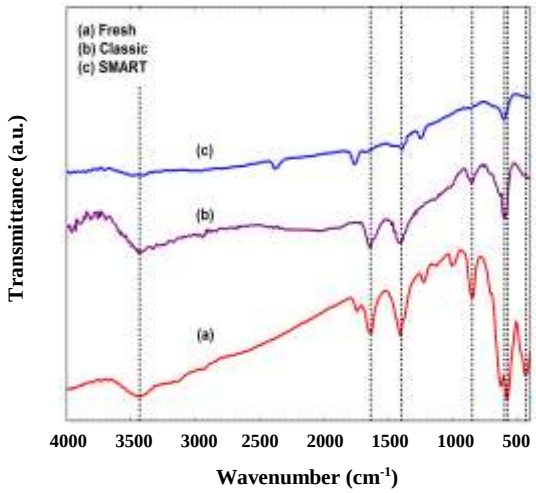

Fig. 4: FT-IR spectrum of fresh and spent catalysts.

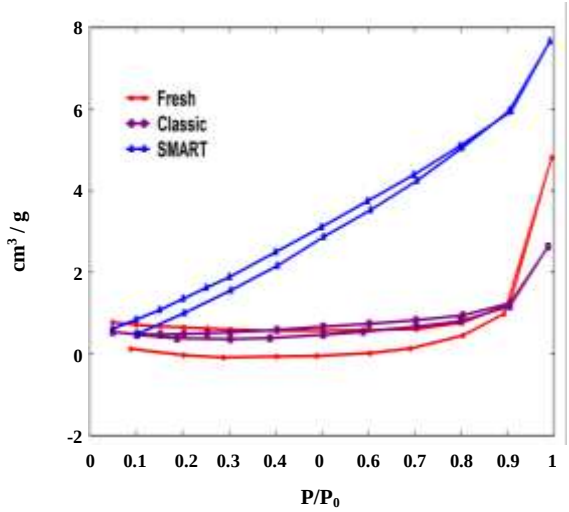

Fig. 5: Adsorption–desorption isotherm for fresh and spent catalysts.

The peaks at 2θ=28.7, 47.44, 56.6 are ascribed to the cubic phase of CeO_2 (JCPDS: 01-075-0076) in the catalysts.

Comparison of Fe_3O_4 crystallite size in spent catalysts indicated more catalyst deactivation in the SMART technology from the conducted XRD analysis. As the structural composition of fresh and spent catalysts shown in Table 3, hexagonal structure of fresh catalyst changed to cubic in the spent ones. In addition, crystallite size increased as a function of particle sintering during operation. It confirms that the SMART spent catalyst undergoes more thermal stress than the classic ones.

Fig. 4 shows FT-IR spectra of fresh and spent catalysts. The bands around 3800 cm^{-1} assigned to stretching vibration due to structural O-H and stretching vibration around 1640 cm^{-1} can be attributed to absorbed water. The peaks at about 430, 577, 840 and 1400 cm^{-1} are corresponding to the Fe-O at Fe_2O_3. However, the observed peak at around 585 cm^{-1} for both spent catalysts is attributed to the Fe-O at Fe_3O_4.

As mentioned before, reduction of Fe^{3+} to Fe^{2+} is classified as catalyst deactivation phenomena in ethylbenzene dehydrogenation which is confirmed by the FT-IR results. Nitrogen adsorption analysis on catalysts was carried out and obtained results are shown in Fig. 5. According to the IUPAC isotherms type II and H1 type hysteresis, observed isotherms for each one of the catalysts is corresponding to nonporous materials larger than microspores [27]. The fresh and spent classic catalysts analysis show almost similar isotherms, while the SMART spent catalyst shows more deviation than the fresh ones.

The catalysts specific surface area was calculated using the BET method which is one of the common techniques for determining catalysts specific surface area. The linear form of BET equation is given as follows:

$$\frac{P}{V_a (p_0 - p)} = \frac{1}{V_{am} C} + \left(\frac{C-1}{V_{am} C} \right) + \frac{p}{p_0} \qquad (9)$$

Table 4: Evaluation of surface area and pore structure of catalysts.

Catalyst	BET Surface Area (m^2/g)	Total Pore Volume (cm^3/g)	Mean Pore Radius (A°)
Fresh	2.04	7.43×10^{-3}	76.84
Spent classic	1.65	4.07×10^{-3}	51.58
Spent SMART	5.28	11.83×10^{-3}	35.82

Where V_a is the amount of adsorbed gas at a relative pressure P/P_0, V_{am} is monolayer adsorption capacity and C is the BET equation constant. The BET points show good linearity for fresh, classic and SMART spent catalysts with correction factors of 0.99, 0.98 and 0.99, respectively. Nitrogen adsorption isotherms results are shown in Table 4.

As can be seen from Table 4, specific surface area and pore volume of the SMART spent catalyst increase to $5.27 m^2/g$ and $11.83 \times 10^{-3} cm^3/g$, respectively which are in contact with the classic spent catalyst behavior. This can be attributed to further potassium migration, followed by the physical changes and pores interconnecting, which is known as transient pores. The average pore radius in both SMART and classic spent catalysts, compared to the fresh one, shows about 53% and 33% reduction, respectively, which could be due to blocked pores mouth resulting from coke and carbonaceous deposits formation. It is believed that styrene is the precursor of coke and carbonaceous deposits formation which resulted in the catalyst activity loss [28, 29].

With respect to pores radius reduction followed by diffusion limitation, the residence time of the reactants at the acid sites and also by-products formation will increase. It is to be expected that the SMART spent catalyst would produce more benzene and toluene compared to the classic ones. By analyzing the DFT cumulative raw data, DFT pore volume histogram of catalysts can be shown in Fig. 6. As can be seen from Fig. 6, the fresh catalyst represents the normal pore size distribution with an equivalent average pore radius 76.84 Å. Due to potassium migration and pore mouth blocking by coke formation, normal pore size distribution disappears in the spent catalysts. The average pore radius in both classic and SMART spent catalysts revealed about 33% and 53% reduction, respectively. The average pore volume increasing along with pore mouth decreasing supports physical degradation and pores interconnection (transient pores) in the SMART spent catalyst.

Fresh and spent catalysts surface were analyzed by SEM-EDX methods. Fig. 7(a) illustrates a SEM microphotograph of the fresh catalyst which has been formed with equal particles sizes distribution. Figs. 7(b) and 7(c) represent the classic and SMART spent catalysts SEM, respectively. It is obvious that the dark grains have been formed on the surface of the spent catalysts and also uniform distribution has disappeared.

Figs. 8 and 9 indicate the chemical composition of the spent catalysts which were analyzed by EDX method. As can be seen, the darker areas contain more potassium than the lighter areas, moreover, the lighter areas posses more iron compared to the darker ones. The obtained results clearly demonstrate that the equal distribution of potassium in the spent catalysts led to more reduction of activity. However, bulk analyzing of both catalysts confirms XRF results (Table 2). Potassium line san was employed to prove the potassium migration or uneven distribution. As results are illustrated in Fig. 10, it can be seen that potassium identically distributed in the radial direction in the fresh catalyst. According to the SEM images, it can be observed that potassium concentration in the spent catalysts is decreased and adequate distribution is vanished. However, based on the SEM results, potassium concentration in the center of the classic spent catalyst is more than that on its surface. These results have been also reported by Mross [11].

According to equations 10 and 11, generated hydrogen causes catalyst deactivation due to the KOH and Fe_3O_4 formation in both technologies. As the melting point of the KOH is 406°C, it would be molten at the reaction temperature. So the Potassium migration towards the center of the classic spent catalyst (intra-particle migration) is attributed to temperature gradient [18]. Moreover, potassium concentration at the surface of the SMART spent catalyst is more than that at its center. This can be associated with potassium migration out of the reactor (inter-particle migration) by chemical vapor transportation via reaction between KOH and CO_2

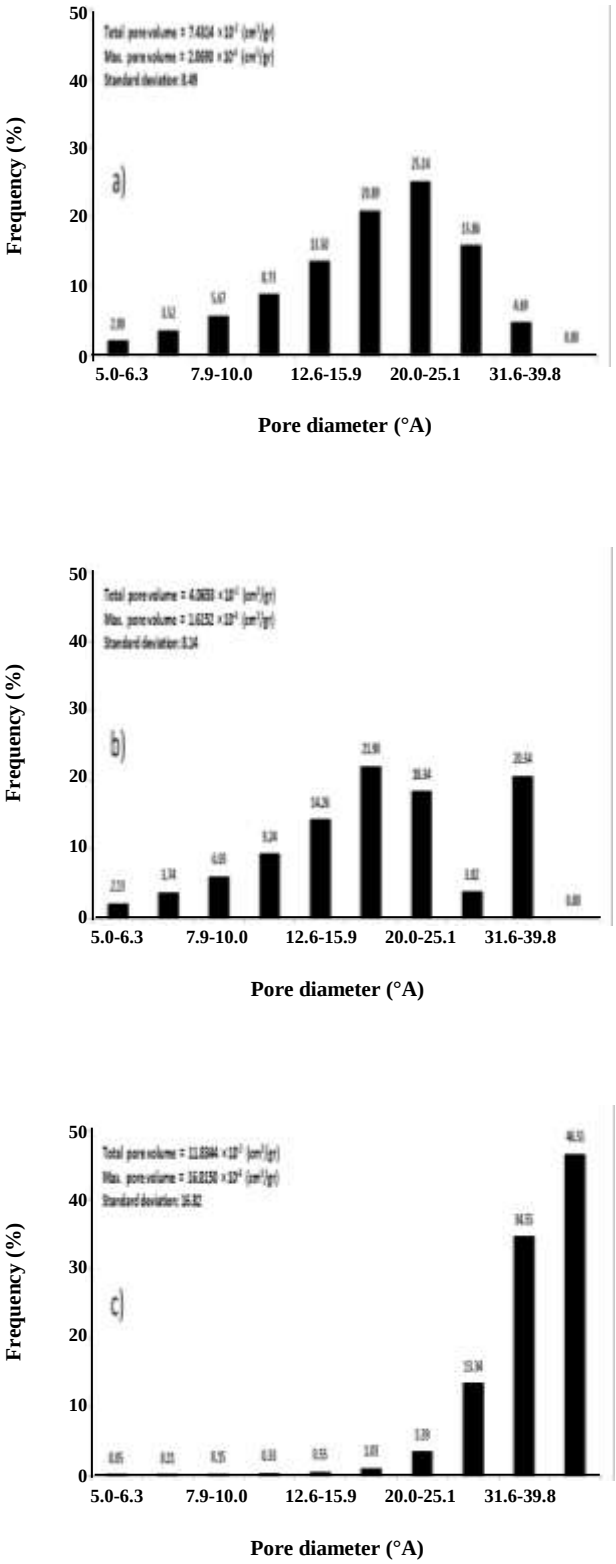

Fig. 6: DFT pore volume histograms of catalysts: (a) fresh, (b) classic spent and (c) SMART spent.

The excess oxygen amount reacts with hydrocarbons and CO_2 is generated in the SMART reactor. According to Eq. 12, generated CO_2 reacts with KOH and K_2CO_3 is formed. It caused downstream pipes clogging due to potassium carbonate sediment build-up which was verified by gradual increasing of pressure drop during operation. However, the high temperature of hydrocarbon oxidation leads to the more thermal stress of catalyst and further KOH melt. So, the center of the SMART spent catalyst is potassium depleted and its concentration on the catalyst surface is very low compared to the fresh ones. Subsequently, the catalyst conversion dropped slowly and a higher level of by-products is formed.

$$3K_2Fe_{22}O_{34} + 11H_2 \rightarrow 6KOH + 22Fe_3O_4 + 8H_2O \quad (10)$$

$$3KFeO_2 + H_2O + (1/2)H_2 \rightarrow 3KOH + Fe_3O_4 \quad (11)$$

$$2KOH + CO_2 \leftrightarrow K_2CO_3 + H_2O \quad (12)$$

Ethylbenzene dehydrogenation is an endothermic reaction and takes place at temperatures of above 580ºC. As well as thermal stress that the dehydrogenation catalyst encounters, the mechanical strength of the catalyst decreases. The gradual reduction of Fe^{3+} to Fe^{2+} leads to the several interrelated deactivation phenomena and mechanical strength drop.

Catalyst crystalline phase transformation from hexagonal in $K_2Fe_{22}O_{34}$ to cubic in Fe_3O_4, confirms a significant change in the mechanical strength. By considering the obtained data from crush strength analysis, it can be seen that fresh catalyst, with approximately 114.6 ± 48.48 N in comparison to the spent catalysts possess high mechanical strength. The mechanical strength of the SMART and classic spent catalysts is 5.5% and 15.5% lower than the fresh ones, respectively. This phenomenon is most obvious during spent catalysts discharge from both classic and SMART reactors.

In addition to the crystalline phase change effects on the mechanical strength, potassium migration leads to change in catalyst density. The mechanical strength reduction and physical degradation cause an increase in pressure drop across the catalyst bed. Subsequently, conversion and selectivity decrease gradually with time in both spent catalysts. The crushing strength distribution histograms of catalyst are shown in Fig. 11.

Activity Tests

The results of the catalytic activity tests of the fresh and spent catalysts are reported in Table 5. The ethylbenzene dehydrogenation over the classic and

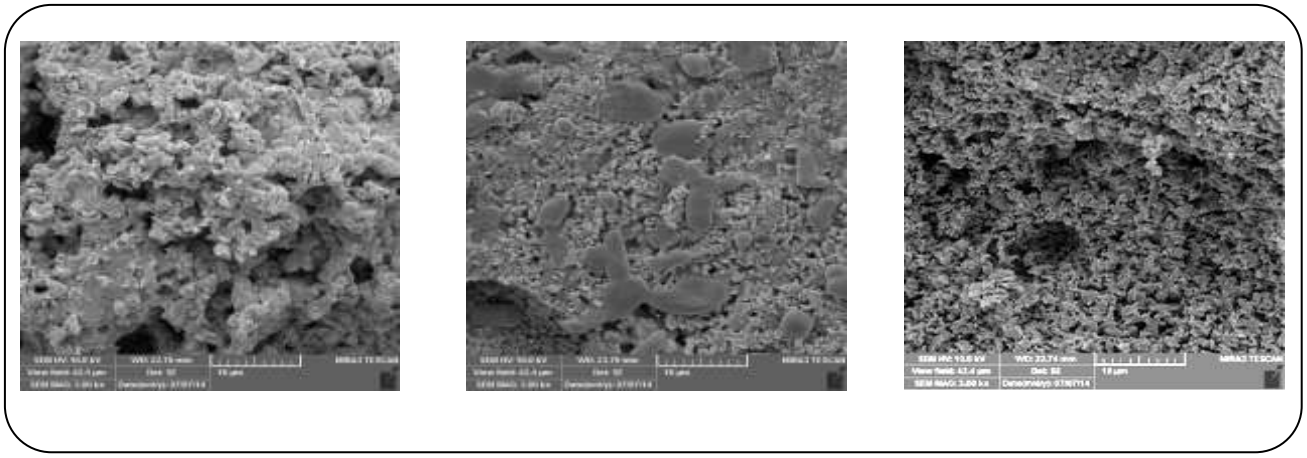

Fig. 7: SEM micrographs of the catalysts: (a) fresh, (b) classic spent and (c) SMART spent.

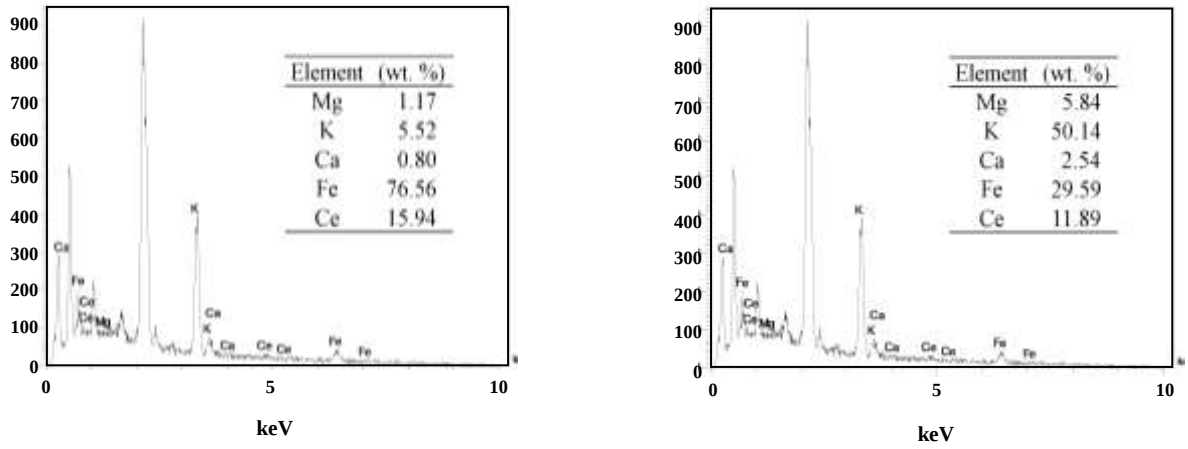

Fig. 8: Chemical composition of light (left) and dark (right) areas of classic spent catalyst performed by EDX.

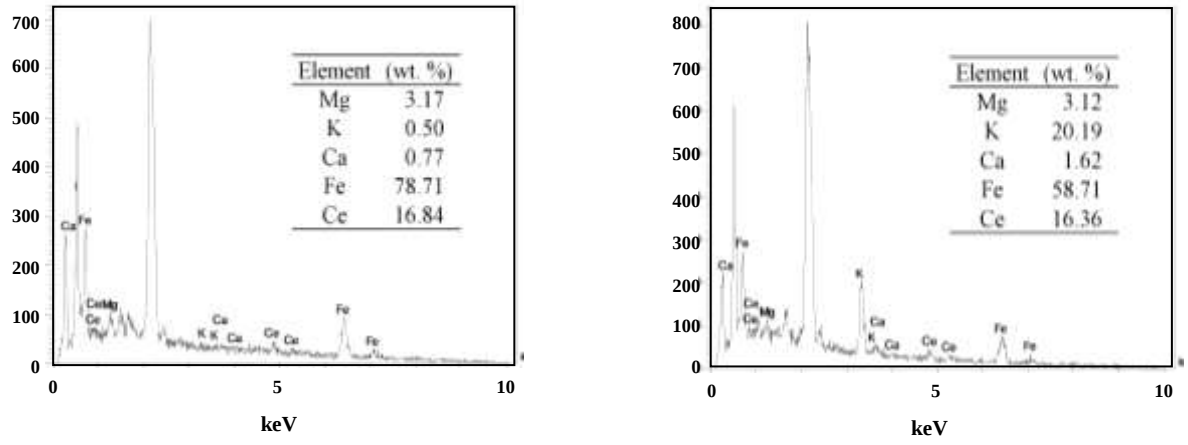

Fig. 9: Chemical composition of light (left) and dark (right) areas of SMART spent catalyst performed by EDX.

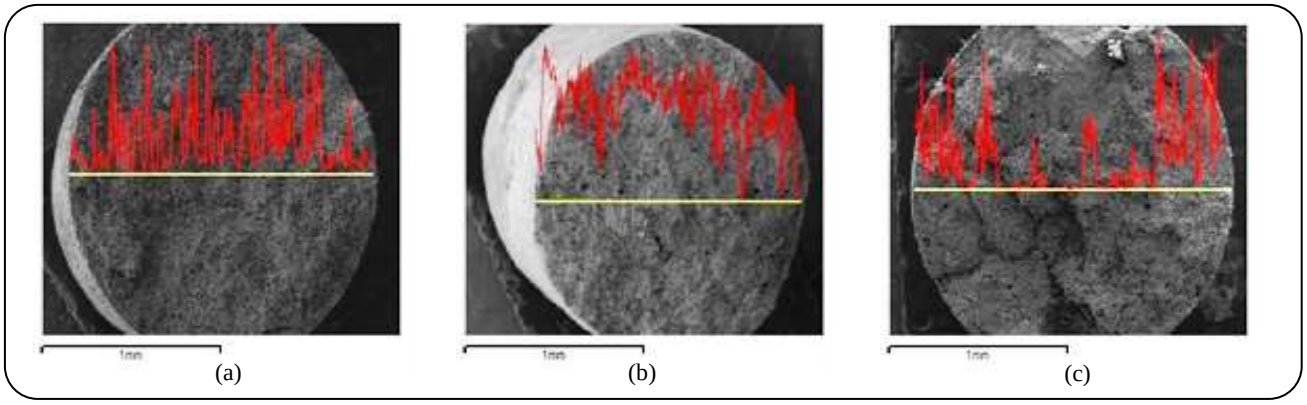

Fig. 10: Potassium line scans of catalyst: (a) fresh, (b) classic spent and (c) SMART spent.

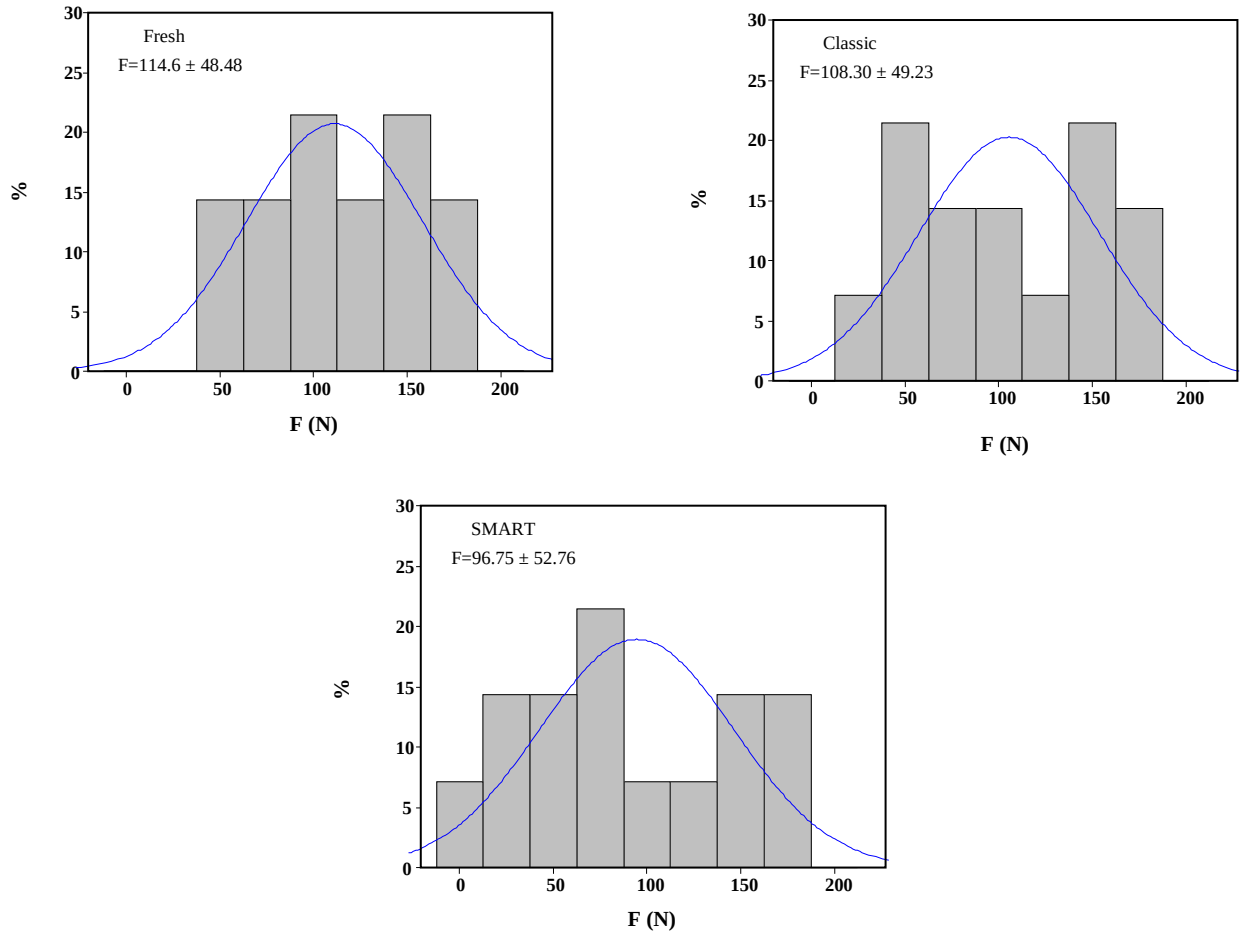

Fig. 11: Crushing strength histograms of catalysts: (a) fresh, (b) classic spent and (c) SMART spent.

SMART spent catalysts indicates that the styrene yield at 640°C is 61 and 72% lower than the fresh ones, respectively. This deviation widens to 74% at 580°C in the SMART spent catalysts. The large drop of the styrene yield (72-74%) of the SMART spent catalyst reveals that the styrene yield is more depending on the pore mouth size, rather than the specific surface area.

Due to the more coke formation resulting from higher volume of potassium migration in the SMART spent catalyst, it can be observed that the cracking reactions

Table 5: Catalytic activity of fresh and spent catalysts at various temperature (S/O=1.3, LHSV=1.0 h^{-1}).

Temperature (°C)	Catalyst	Ethylbenzene Conversion	Styrene Selectivity	Benzene Selectivity	Toluene Selectivity	Styrene Yield
580	Fresh	37.73	79.05	13.20	8.96	29.82
	Spent classic	18.37	63.86	18.26	11.15	11.73
	Spent SMART	15.41	51.28	18.50	12.05	7.90
640	Fresh	54.38	76.04	15.31	9.83	41.35
	Spent classic	29.13	55.29	18.91	13.62	16.10
	Spent SMART	26.57	44.02	19.28	14.19	11.70

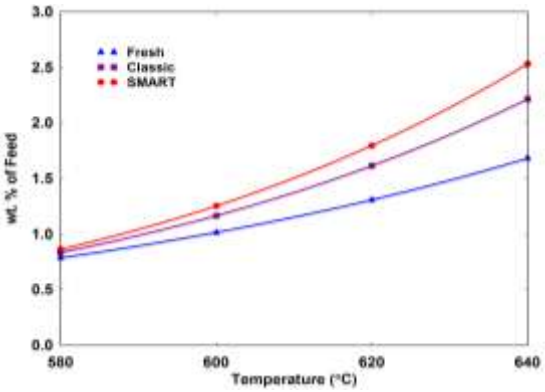

Fig. 12: Inlet feed converted to off-gas (%) for fresh and spent catalysts (S/O=1.3, LHSV=1.0 h^{-1}).

are also increased. However, the sharp drop in styrene yield for both spent catalysts verifies that the catalytic activity on the carbon surface is lower than the $KFeO_2$ phase. It is believed that the ethylbenzene dehydrogenation to styrene can perform on both carbon and $KFeO_2$ surface [22].

The off gas production is one of the undesirable results of the catalysts performance, in line with the following equations [5].

$$H_2O + 1/2\ C_2H_4 \longrightarrow CO + 2H_2 \qquad (13)$$
$$\Delta H = 225.6\,kJ/mol$$

$$H_2O + CH_4 \longrightarrow CO + 3H_2 \qquad (14)$$
$$\Delta H = 216.2\,kJ/mol$$

$$H_2O + CO \longrightarrow CO_2 + H_2 \qquad (15)$$
$$\Delta H = -42.1\,kJ/mol$$

The weight percentage of ethylbenzene feed converted to the off gas during the dehydrogenation reaction is depicted in Fig. 12. As can be observed, all of the catalysts showed almost identical off gas production at 580°C. Furthermore, according to Eqs. (13-15), off gas production elevates the partial pressures of reactants and decreases the styrene production.

The gradual temperature rise during the operation time indicates that the most of the off gas production is associated with the SMART spent catalyst. The activity test results clearly demonstrate that the off gas production on carbon surface is higher than the $KFeO_2$ phase.

As steam injection redistributes migrated potassium [12], in situ steam injection was carried out and activity tests were performed for both of the spent catalysts. According to the reported results in Table 6, the classic and SMART spent catalysts conversion increase by 9.31% and 4.47%, respectively. This can be attributed to the partial coke gasification by steam which is known as a soft oxidizing agent.

However, the selectivity of the classic spent catalyst rises by a 2.18. It can be associated with potassium redistribution from the center toward the surface of the catalyst [12]. So, steam injection causes an identical redistribution of potassium in the classic spent catalyst and increases styrene selectivity. Despite, steam injection drops the selectivity of the SMART spent catalyst by a 0.41%. According to potassium depletion from the center and high level of its concentration at the surface of the SMART spent catalyst, steam injection leads to more potassium migration out of the catalyst by chemical vapor transportation (inter-particle migration).

CONCLUSIONS

The evaluation of spent catalyst structure changes during ethylbenzene dehydrogenation in different technologies has been studied. The results show that high rate of potassium migration depends on styrene production method. So that the styrene production via

Table 6: Changes in spent catalysts activity after 30 min steam injection. (T=580 °C, S/O=1.3, LHSV=1.0 hr^{-1}).

Spent catalyst	Original (as received)		After steam treatment		% Change	
	Conversion	Selectivity	Conversion	Selectivity	Conversion	Selectivity
Classic	18.37	63.86	20.08	65.25	9.31	2.18
SMART	15.41	51.28	16.10	51.07	4.47	-0.41

classic and SMART technologies by 26 and 40% potassium loss, leads to more catalyst deactivation than the fresh ones, respectively. In addition, the pore structure analysis revealed that the mean pore size reduction along with diffusion limitation in the SMART technology causes an increase in residence time of reactants and by-products formation.

Moreover, potassium migration in the classic spent catalyst is attributed to the temperature gradient and it is directed towards the center of the catalyst (intra-particle potassium migration). Unlike, the chemical reaction results in a change in the potassium migration pattern towards the out of the catalyst in the SMART spent catalyst (inter-particle chemical vapor transportation). Furthermore, in situ steam injection redistributes migrated potassium in the classic spent catalyst and the selectivity of the catalysts increases. But it leads to more potassium migration and higher selectivity drop in the SMART spent ones.

Generally, it can be said that excess oxygen injection changes catalysts deactivation mechanism and accelerates potassium migration and catalyst deactivation in the SMART technology. Generally, it can be concluded that the styrene production through SMART technology has more disadvantages and industrial unit designing based on it not recommended strongly.

Acknowledgment

The authors would like to thank Sahand University of Technology (SUT) and Environmental Engineering Research Center (EERC) for their support for this research work.

Received: Jul. 25, 2015 ; Accepted: Jun. 1, 2016

REFERENCES

[1] James D.H., Castor W.M., "Ullmann's Encyclopedia of Industrial Chemistry", Wiley-VCH Verlag GmbH & Co., Weinheim (2011).

[2] Scheirs J., Priddy D., "Modern Styrenic Polymers", John Wiley & Sons, Weinheim (2003).

[3] Tamsilian Y., Ebrahimi A.N., Ramazani A., Abdollahzadeh H., Modeling and Sensitivity Analysis of Styrene Monomer Production Process and Investigation of Catalyst Behavior, *Comput. Chem. Eng.*, **40**(1):1-11 (2012).

[4] Jafarzadeh Y., Shafiei S., Ebadi A., Abdoli M., Batch Separation of Styrene/Ethylbenzene/Water Dispersions, *Iran. J. Chem. Eng.(IJChE)*, **7**(4):22-28 (2010).

[5] Cavani F., Trifiro F., Alternative Processes for the Production of Styrene, *Appl. Catal. A.: General*, **133**(2):219-239 (1995).

[6] Arpe H.J., "Industrial Organic Chemistry", Wiley-VCH Verlag GmbH & Co., Weinheim (2010).

[7] Khatamian M., Khandar A.A., Haghighi M., Ghadiri M., Nano ZSM-5 Type Ferrisilicates as Novel Catalysts for Ethylbenzene Dehydrogenation in the Presence of N_2O, *Appl. Surf. Sci.*, **258**(2):865-872 (2011).

[8] Castro A.J.R., Soares J.M., Filho J.M., Oliveira A.C., Campos A., Milet E.R.C., Oxidative Dehydrogenation of Ethylbenzene with CO_2 for Styrene Production over Porous Iron-based Catalysts, *Fuel*, **108**(1):740-748 (2013).

[9] Humin Y., Hong L., Jilong W., Tao W., Wenjun Y., Xiaoli H., Jiejun B., Guoping X., Development Status of Ethylbenzene Dehydrogenation Catalysts, *Ind. Catal.*, **20**(1):13-18 (2012).

[10] Tahriri-Zangeneh F., Taeb A., Gholivand K., Sahebdelfar S., The Effect of Alkali Metal Promoters on the Stability and Coke Formation of Platinum-Based Propane Dehydrogenation Catalysts: A Kinetic Study, *Iran. J. Chem. Chem. Eng.(IJCCE)*, **32**(4):25-32 (2013).

[11] Mross W.D., Alkali Doping in Heterogeneous Catalysis, *Cataly. Rev.*, **25**(4):591-637 (1983).

[12] Herzogt, B.D., Rase, H.F., In Situ Catalyst Reactivation: Spent Ethylbenzene Catalyst with Agglomerated Potassium Promoter, *Ind. Eng. Chem. Dev.*, **23**(2):187-196 (1984).

[13] Matsui J., Sodesawa T., Nozaki F., Activity Decay of Potassium-Promoted Iron Oxide Catalyst for Dehydrogenation of Ethylbenzene, *Appl. Catal. A.: General*, **51**(1):203-211 (1989).

[14] Matsui J., Sodesawa T., Nozaki, F., Influence of Carbon Dioxide Addition upon Decay of Activity of a Potassium-Promoted Iron Oxide Catalyst for Dehydrogenation of Ethylbenzene. *Appl. Catal. A.: General*, **67**(1):179-188 (1990).

[15] Serafin I., Kotarba A., Grzywa M., Sojka Z., Binczycka H. Kustrowski P., Quenching of Potassium Loss from Styrene Catalyst: Effect of Cr Doping on Stabilization of the $K_2Fe_{22}O_{34}$ Active Phase, *J. Catal.*, **239**(1):137-144 (2006).

[16] Bieniasz W., Trebala M., Sojka Z., Kotarba A., Irreversible Deactivation of Styrene Catalyst due to Potassium Loss—Development of Antidote via Mechanism Pinning, *Catal. Today*, **154**(3-4):224-228 (2010).

[17] Rossetti I., Bencini E., Trentini L., Forni, L., Study of the Deactivation of a Commercial Catalyst for Ethylbenzene Dehydrogenation to Styrene, *Appl. Catal. A.: General*, **292**(1):118-123 (2005).

[18] Meima G.R., Menon P.G., Catalyst Deactivation Phenomena in Styrene Production, *Appl. Catal. A.: General*, **212**(1-2):239-245 (2001).

[19] Mousavi S., Panahi P., Niaei A., Modeling and Simulation of Styrene Monomer Reactor: Mathematical and Artificial Neural Network Model, *Int. J. Sci. Eng. Res.(IJSER)*, **3**(3):1-7 (2012).

[20] Aghayarzadeh M., Alizadeh R., Shafiei S., Simulation and Optimization of Styrene Monomer Production using Neural Network, *Iran. J. Chem. Eng.(IJChE)*, **11**(1):30-41 (2014).

[21] Lee W.J., Froment G.F., Ethylbenzene Dehydrogenation into Styrene: Kinetic Modeling and Reactor Simulation, *Ind. Eng. Chem. Res.*, **47**(23):9183-9194 (2008).

[22] Baghalha M., Ebrahimpour O., Structural Changes and Surface Activities of Ethylbenzene Dehydrogenation Catalysts during Deactivation, *Appl. Catal. A: General*, **326**(2):143-151 (2007).

[23] Shijie L., Tong C., Changxi M., Weimin Y., Zaiku X., Qingling C., Deactivation of the Industrial Catalyst for Ethylbenzene Dehydrogenation to Styrene, *Chinese J. Catal.*, **29**(2):179-184 (2008).

[24] Muhler M., Schutze J., Wesemann M., Rayment T., Dent A., Schlogl R. Ertl G., The Nature of the Iron Oxide-based Catalyst for Dehydrogenation of Ethylbenzene to Styrene: I. Solid-state Chemistry and Bulk Characterization, *J. Catal.*, **126**(2):339-360 (1990).

[25] Ndlela S.C., Shanks B.H., Reducibility of Potassium-Promoted Iron Oxide under Hydrogen Conditions, *Ind. Eng. Chem. Res.*, **42**(10):2112-2121 (2003).

[26] Subrt J., Vins J., Shapygin I.S., Zakharov A.A., Reactivity of Finely Dispersed Iron Oxides in Solid State Reactions, *Thermochim. Acta.*, **93**(1):489-492 (1985).

[27] Gregg S.J., Sing K.S.W., "Adsorption, Surface Area, and Porosity", Academic Press, London (1995).

[28] Kopinke F.D., Zimmermann G., Reyniers G., Froment G.F., Relative Rates of Coke Formation from Hydrocarbons in Steam Cracking of Naphtha. 3. Aromatic Hydrocarbons, *Ind. Eng. Chem. Res.*, **32**(11):2620-2625 (1993).

[29] Guisnet M., Magnoux P., Organic Chemistry of Coke Formation, *Appl. Catal. A: General*, **212**(1-2): 83-96 (2001).